Available online at www.sciencedirect.com
ScienceDirect
International Journal of Heat and Mass Transfer 51 (2008) 1530–1541
International Journal of HEAT and MASS TRANSFER
www.elsevier.com/locate/ijhmt

Nonlinear thermal optimization of external light concrete multi-holed brick walls by the finite element method

J.J. del Coz Díaz [a,*], P.J. García Nieto [b], J.L. Suárez Sierra [a], C. Betegón Biempica [a]

[a] Department Building of Viesques, N° 7-33204 Gijón (Asturias), Spain
[b] Department of Mathematics, Faculty of Sciences, C/ Calvo Sotelo s/n – 33007 Oviedo (Asturias), Spain

Received 16 April 2007
Available online 12 September 2007

Abstract

In this work, an analysis and numerical study have been carried out in order to determine the best candidate brick from the thermal point of view by the finite element method. With respect to the ecological design and the energy saving for housing and industrial structures, there is also a great interest in light building materials with good physical and thermal behaviours, which fulfils all thermal requirements of the new CTE Spanish rule for further energy savings. The conduction, convection and radiation phenomena are taking into account in this study for four different types of bricks varying the material conductivity obtained from the experimental tests. Based on the previous thermal analysis, the best candidate was chosen and then a full $1.05 \times 0.35 \times 1.0$ m. wall made of these bricks was simulated for fifteen different compositions and temperature distribution is also provided for some typical configurations. The major variables influencing the thermal conductivity of these walls are illustrated in this work for different concrete and mortar properties. The finite element method (FEM) is used for finding accurate solutions of the heat transfer equation for light concrete hollow brick walls. Mathematically, the nonlinearity is due to the radiation boundary condition inside the inner recesses of the bricks. Optimization of the walls is carried out from the finite element analysis of four hollow brick geometries by means of the average mass overall thermal efficiency and the equivalent thermal conductivity. In order to select the appropriate wall satisfying the CTE requirements, detailed instructions are given. Finally, conclusions of this work are exposed.

Keywords: External hollow brick wall; Light concrete; Finite element modelling; Nonlinear complex heat transfer; Energy savings; Thermal optimization

1. Introduction

The Kyoto Protocol is an agreement made under the United Nations Framework Convention on Climate Change (UNFCCC). Countries that ratify this protocol, including Spain, commit to reduce their emissions of carbon dioxide and five other greenhouse gases, or engage in emissions trading if they maintain or increase emissions of these gases. This Protocol now covers more than 160 countries globally and over 55% of global greenhouse gas (GHG) emissions.

These government organizations are working closely with their major utility, energy, oil and gas and chemicals conglomerates in order to decrease the GHG emissions. At present time, energy consumption of buildings in Spain and other States of the European Union (EU) is a high-priority subject. For this reason the buildings sector has been studied as part of a broader examination in relation to a rational fuel use and emissions in Spain and the rest of the EU countries. Our aim is the reduction of the energy consumption in the Spanish buildings for the best thermal protection of the external enclosure.

The thermal conditions for the Spanish buildings are defined at present by the new Building Standard Code (named CTE project [1]). This rule modifies the previous Spanish rule, the oldest rule of Europe, completely obsolete

* Corresponding author. Tel.: +34 985182042; fax: +34 985 182433.
E-mail address: juanjo@constru.uniovi.es (J.J.d. Coz Díaz).

0017-9310/$ - see front matter © 2007 Elsevier Ltd. All rights reserved.
doi:10.1016/j.ijheatmasstransfer.2007.07.029

Nomenclature

A	surface area of the body through which heat flows (m^2)
c	specific heat of the material (J/(kg K))
CSI	climate severity index (dimensionless)
E	thickness of the brick (m)
$e_{thermal\_p}$	mass overall thermal efficiency in percentage (m^2 K/W/kg)
h	heat transfer coefficient or film coefficient (W/(m^2 K))
h_r	radiation heat transfer coefficient (W/(m^2 K))
k	thermal conductivity of the material (W/(m K))
k_x	thermal conductivity of the material in x-direction (W/(m K))
l_x, l_y, l_z	direction cosines of the outward drawn normal to the boundary
M	mass (kg)
R_{tot}	overall thermal resistance of the wall, taking into account the corrections due to moisture and holes, and film coefficients (m^2 K/W)
R_{si}	internal surface resistance of the wall (m^2 K/W)
R_{se}	external surface resistance of the wall (m^2 K/W)
S_1	boundary on which the value of temperature is specified as $T_0(t)$ (Dirichlet condition)
S_2	boundary on which the heat flow q is specified (Neumann condition)
S_3	boundary on which the convective heat loss $h(T - T_\infty)$ is specified (convective Neumann condition)
T	temperature of the body or surface temperature (K)
$\bar{T}_0$	specified temperature distribution at time zero (K)
T_∞	temperature of the surrounding medium (K)
ΔT	difference of temperature (K)
t	time parameter (s)
q	rate of heat flow or heat flux (W/m^2)
$\dot{q}$	strength of the heat source (rate of heat generated per unit volume per unit time) (W/m^3)
U_{wall}	thermal transmittance (W/m^2 K)
U	overall heat transfer coefficient (W/m^2 K)
V	volume of the body (m^3)
x	length parameter (m)
σ	Stefan–Boltzmann constant ($=5.67 \times 10^{-8}$ W/m^2 K^4)
ε	emissivity of the surface (dimensionless and $\varepsilon = 0.85$)
ρ	density of the material (kg/m^3)
λ_t	real conductivity of the material obtained in tests (W/m K)
λ_e	estimated conductivity of the brick from the fitting data (W/m K)
λ_{mortar}	conductivity of the mortar (W/m K)
$\lambda_{equivalent}$	equivalent thermal conductivity (W/m K)

from the technical point of view, since it allowed very high energy consumptions and it did not meet all the current demands of the Spanish society in this aspect.

The CTE rule, in its requirement of habitability and energy saving, introduces modifications that improve the scarce requirements of the same one by means of improvement of thermal insulation of the building's enclosure.

However, the CTE rule does not totally take advantage of the different possibilities of decrease of the energy needs of a building. It is possible to show that we can increase the capacity of insulation in the facades of the buildings (both in walls and in glass rooms) beyond the prescribed one in the CTE project, keeping a good profitability of the investment.

The energy demand of buildings in the CTE rule is limited depending on the city climate and the internal load in their rooms. In order to calculate the different climatic zones inside a country, it is necessary to know climatic data of the same. The determination of climatic zones is obtained from the climate severity index (CSI), both in winter and in summer seasons. The CSI combines the degree-day and the solar radiation of the city, so that when two towns have the same winter CSI the energy consumption of the same building is almost equal. The same consideration is applied to the summer CSI. There are five different climatic zones in winter (A, B, C, D and E) and four in summer (1, 2, 3 and 4), according to Tables 1 and 2.

In order to avoid decompensations between the thermal qualities of different rooms, each one of internal and external walls of thermal enclosure will have a transmittance lower than the values shown in Table 3.

Table 1
Climatic severity indexes for winter

A	B	C	D	E
CSI = 0.3	0.3 < CSI ⩽ 0.6	0.6 < CSI ⩽ 0.95	0.95 < CSI ⩽ 1.3	CSI > 1.3

Table 2
Climatic severity indexes for summer

1	2	3	4
CSI = 0.6	0.6 < CSI ⩽ 0.9	0.9 < CSI ⩽ 1.25	CSI > 1.25

Table 3
Maximum thermal transmittance of external walls

Climatic zone	Thermal transmittance U_{wall} [W/m^{2}K]
A3	0.93
A4	0.94
B3 and B4	0.82
C1, C2, C3 and C4	0.73
D1, D2 and D3	0.66
E1	0.57

2. Geometry and shape variables

In the first place, we have modeled four different types of light concrete hollow bricks (see Fig. 1 below) designed according to the performance of the brick's previous model M1 [2,3] in order to improve the thermal behavior of the same ones [4,5] following the requirements of the new CTE Rule [1].

Just as it is shown in Fig. 1, the four types of bricks (*N*1, *N*2, *N*3 and *N*4) have the same external dimensions. These dimensions will be kept constant in the calculation and the subsequent optimization process due to ergonomic reasons. The human body's response to physical loads in the building of the wall is strongly related to the total mass of the brick. This last requirement limits the external maximum dimensions of the brick's design to the values previously indicated above.

The main differences between them are focused on two important aspects:

(1) The shape and dimensions of the central recesses.
(2) The length of the recesses in the longitudinal direction.

For instance, bricks *N*2 and *N*4 are very similar with respect to the shape of the recesses. The difference between them is the length of all the recesses. However, bricks *N*1, *N*2 and *N*3 are only different with respect to the shape and dimensions of the central recesses.

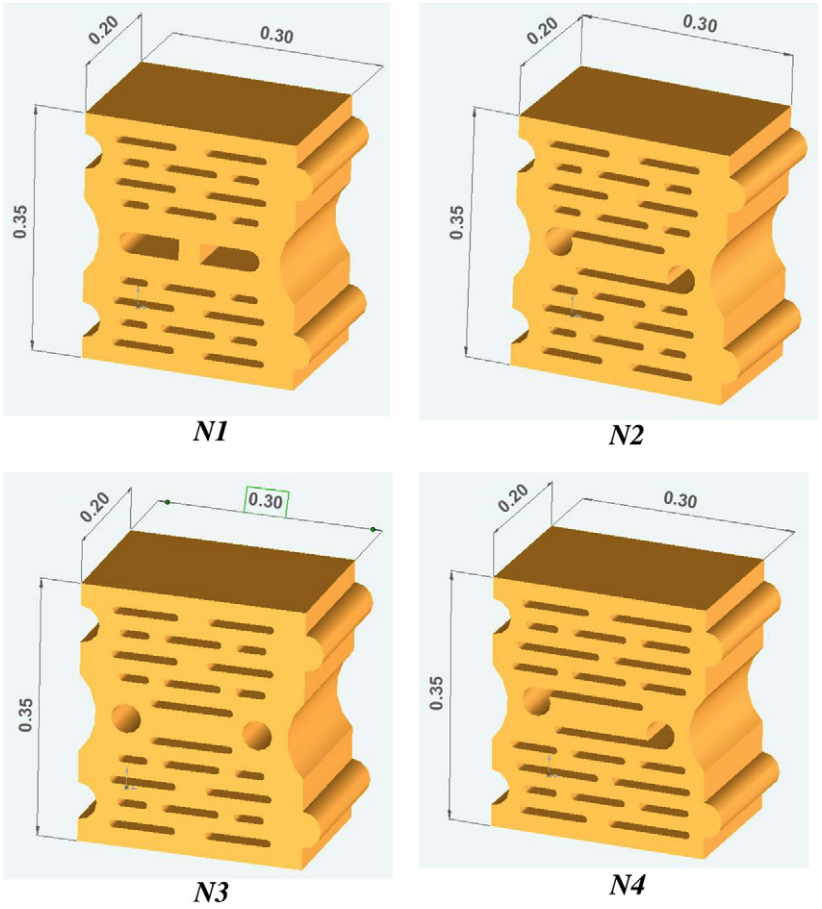

Fig. 1. Geometrical model and dimensions (long × width × high) of the bricks *N*1, *N*2, *N*3, and *N*4: 0.3 × 0.35 × 0.19 m.

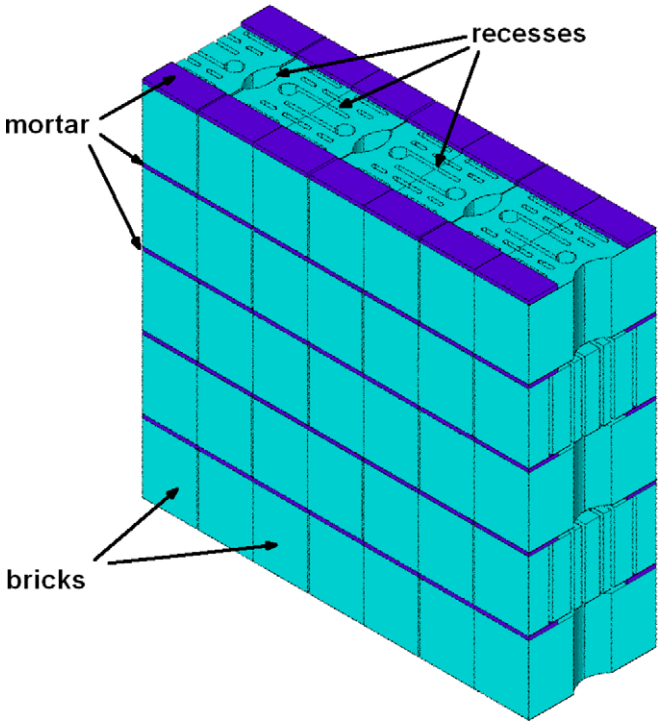

Fig. 2. Geometrical model of a wall composed of bricks *N*2.

Secondly, the wall is composed of 25 bricks and six halves at half must, joined to each other by a half layer mortar of 0.01 m high and 0.08 m width. The overall dimensions of the wall are 1.05 × 0.35 × 1.0 m. (see Fig. 2).

3. Mathematical model of heat equation

3.1. Boundary and initial conditions

Since the governing differential equation of heat transfer is second-order in space, two boundary conditions need to be specified. The possible boundary conditions are (see Fig. 3) [6–9]:

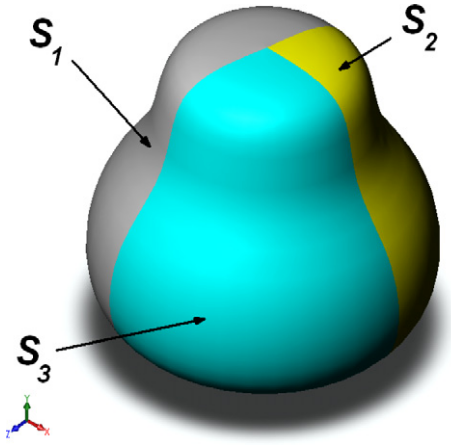

Fig. 3. Three-dimensional model with boundary conditions.

$$T(x,y,z,t) = T_0 \quad \text{for } t > 0 \quad \text{on } S_1 \tag{1}$$

$$k_x \frac{\partial T}{\partial x} l_x + k_y \frac{\partial T}{\partial y} l_y + k_z \frac{\partial T}{\partial z} l_z + q = 0 \quad \text{for } t > 0 \quad \text{on } S_2 \tag{2}$$

and

$$k_x \frac{\partial T}{\partial x} l_x + k_y \frac{\partial T}{\partial y} l_y + k_z \frac{\partial T}{\partial z} l_z + h(T - T_\infty) = 0 \quad \text{for } t > 0 \quad \text{on } S_3 \tag{3}$$

Further the differential equation of heat transfer is first-order in time t and hence it requires one initial condition. The commonly used initial condition is

$$T(x,y,z,t=0) = \bar{T}_0(x,y,z) \quad \text{in } V \tag{4}$$

3.2. Variational or weak formulation of the problem

Thus the problem of finding the temperature distribution inside a solid body involves the solution of heat transfer equation subject to the satisfaction of the boundary conditions of Eqs. (1)–(3) and the initial condition given by Eq. (4).

The three-dimensional heat conduction problem can be stated in an equivalent variational form as follows [10]:

"Find the temperature distribution $T(x, y, z, t)$ inside the solid body which minimizes the integral:

$$I = \frac{1}{2}\int_V \left[k_x \left(\frac{\partial T}{\partial x}\right)^2 + k_y \left(\frac{\partial T}{\partial y}\right)^2 + k_z \left(\frac{\partial T}{\partial z}\right)^2 + 2\left(\dot{q} - \rho c \frac{\partial T}{\partial t}\right) T \right] \mathrm{d}V \tag{5}$$

and satisfies the boundary conditions of Eqs. (1)–(3) as well as the initial condition of Eq. (4)".

Generally it is not difficult to satisfy the boundary condition of Eq. (1), but Eqs. (2) and (3) present some difficulty. To overcome this difficulty, an integral pertaining to the boundary conditions of Eqs. (2) and (3) is added to the functional of Eq. (5) so that when the combined functional is minimized, the boundary conditions of Eqs. (2) and (3) would be automatically satisfied. The integral pertaining to Eqs. (2) and (3) is given by

$$I = \frac{1}{2}\int_V \left[k_x \left(\frac{\partial T}{\partial x}\right)^2 + k_y \left(\frac{\partial T}{\partial y}\right)^2 + k_z \left(\frac{\partial T}{\partial z}\right)^2 + 2\left(\dot{q} - \rho c \frac{\partial T}{\partial t}\right) T \right] \mathrm{d}V + \int_{S_2} qT \,\mathrm{d}S_2 + \frac{1}{2}\int_{S_3} h(T - T_\infty)^2 \mathrm{d}S_3 \tag{6}$$

3.3. Galerkin finite element approach

The finite element procedure using Galerkin method can be described by the following steps [11,12]:

- *Step 1*: Divide the domain V into E finite elements of p nodes each.
- *Step 2*: Assume a suitable form of variation of T in each finite element and express $T^{(e)}(x,y,z,t)$ in element e as

$$T^{(e)}(x,y,z,t) = [N(x,y,z)]\vec{T}^{(e)} \tag{7}$$

where

$$[N(x,y,z)] = [N_1(x,y,z), N_2(x,y,z), \ldots, N_p(x,y,z)]$$

and

$$\vec{T}^{(e)} = \{T_1(t), T_2(t), \ldots, T_p(t)\}^{(e)T}$$

with $T_i(t)$ denoting the temperature of node i and $N_i(x,y,z)$ the interpolation function corresponding to node i of element e.

- *Step 3*: In Galerkin method, the integral of the weighted residue over the domain of the element is set equal to zero by taking the weights same as the interpolation functions N_i. Since the solution of Eq. (6) is not exact, substitution of Eq. (7) into the differential equation of heat transfer gives a nonzero value instead of zero. This nonzero value will be the residue. Hence the criterion to be satisfied at any instant of time is

$$\int_{V^{(e)}} N_i \left[\frac{\partial}{\partial x}\left(k_x \frac{\partial T^{(e)}}{\partial x}\right) + \frac{\partial}{\partial y}\left(k_y \frac{\partial T^{(e)}}{\partial y}\right) + \frac{\partial}{\partial z}\left(k_z \frac{\partial T^{(e)}}{\partial z}\right) + \dot{q} - \rho c \frac{\partial T^{(e)}}{\partial t}\right] dV = 0, \quad i = 1,2,\ldots,p \tag{8}$$

By noting that the first integral term of Eq. (8) can be written as

$$\int_{V^{(e)}} N_i \frac{\partial}{\partial x}\left(k_x \frac{\partial T^{(e)}}{\partial x}\right) dV = -\int_{V^{(e)}} \frac{\partial N_i}{\partial x} k_x \frac{\partial T^{(e)}}{\partial x} dV + \int_{S^{(e)}} N_i k_x \frac{\partial T^{(e)}}{\partial x} l_x \, dS \tag{9}$$

and with similar expressions for the second and third integral terms, Eq. (8) can be stated as

$$-\int_{V^{(e)}} \left[k_x \frac{\partial N_i}{\partial x}\frac{\partial T^{(e)}}{\partial x} + k_y \frac{\partial N_i}{\partial y}\frac{\partial T^{(e)}}{\partial y} + k_z \frac{\partial N_i}{\partial z}\frac{\partial T^{(e)}}{\partial z}\right] dV + \int_{S^{(e)}} N_i \left[k_x \frac{\partial T^{(e)}}{\partial x} l_x + k_y \frac{\partial T^{(e)}}{\partial y} l_y + k_z \frac{\partial T^{(e)}}{\partial z} l_z\right] dS + \int_{V^{(e)}} N_i \left(\dot{q} - \rho c \frac{\partial T^{(e)}}{\partial t}\right) dV = 0, \quad i = 1,2,\ldots,p \tag{10}$$

Since the boundary of the element $S^{(e)}$ is composed of $S_1^{(e)}$, $S_2^{(e)}$ and $S_3^{(e)}$, the surface integral of Eq. (10) over $S_1^{(e)}$ would be zero (since $T^{(e)}$ is prescribed to be a constant T_0 on side $S_1^{(e)}$, the derivatives of $T^{(e)}$ with respect to x, y and z would be zero). On the surfaces $S_2^{(e)}$ and $S_3^{(e)}$, the boundary conditions given by Eqs. (2) and (3) are to be satisfied. For this, the surface integral in Eq. (10) over $S_2^{(e)}$ and $S_3^{(e)}$ are written in equivalent form as [11,13]

$$\int_{S_2^{(e)}+S_3^{(e)}} N_i \left[k_x \frac{\partial T^{(e)}}{\partial x} l_x + k_y \frac{\partial T^{(e)}}{\partial y} l_y + k_z \frac{\partial T^{(e)}}{\partial z} l_z\right] dS = -\int_{S_2^{(e)}} N_i q \, dS_2 - \int_{S_3^{(e)}} h_i \left(T^{(e)} - T_\infty\right) dS_3 \tag{11}$$

By using Eqs. (6) and (11), Eq. (11) can be expressed in matrix form as

$$[K_1^{(e)}]\vec{T}^{(e)} + [K_2^{(e)}]\vec{T}^{(e)} + [K_3^{(e)}]\dot{\vec{T}}^{(e)} - \vec{P}^{(e)} = \vec{0} \tag{12}$$

where the elements of the matrices are given by

$$K_{1\,ij}^{(e)} = \int_{V^{(e)}} \left(k_x \frac{\partial N_i}{\partial x}\frac{\partial N_j}{\partial x} + k_y \frac{\partial N_i}{\partial y}\frac{\partial N_j}{\partial y} + k_z \frac{\partial N_i}{\partial z}\frac{\partial N_j}{\partial z}\right) dV \tag{13}$$

$$K_{2\,ij}^{(e)} = \int_{S_3^{(e)}} h N_i N_j \, dS_3 \tag{14}$$

$$K_{3\,ij}^{(e)} = \int_{V^{(e)}} \rho c N_i N_j \, dV \tag{15}$$

and

$$P_i^{(e)} = \int_{V^{(e)}} \dot{q} N_i \, dV - \int_{S_2^{(e)}} q N_i \, dS_2 + \int_{S_3^{(e)}} h T_\infty N_i \, dS_3 \tag{16}$$

The previous expressions (13)–(16) can also be given in matrix notation as

$$[K_1^{(e)}] = \int_{V^{(e)}} [B]^T [D][B] dV \tag{17}$$

$$[K_2^{(e)}] = \int_{S_3^{(e)}} h[N]^T [N] dS_3 \tag{18}$$

$$[K_3^{(e)}] = \int_{V^{(e)}} \rho c [N]^T [N] dV \tag{19}$$

$$\vec{P}^{(e)} = \vec{P}_1^{(e)} - \vec{P}_2^{(e)} + \vec{P}_3^{(e)} \tag{20}$$

where

$$\vec{P}_1^{(e)} = \int_{V^{(e)}} \dot{q}[N]^T dV$$

$$\vec{P}_2^{(e)} = \int_{S_2^{(e)}} q[N]^T dS_2$$

$$\vec{P}_3^{(e)} = \int_{S_3^{(e)}} h T_\infty [N]^T dS_3 \tag{21}$$

$$[D] = \begin{bmatrix} k_x & 0 & 0 \\ 0 & k_y & 0 \\ 0 & 0 & k_z \end{bmatrix}$$

and

$$[B] = \begin{bmatrix} \frac{\partial N_1}{\partial x} & \frac{\partial N_2}{\partial x} & \cdots & \frac{\partial N_p}{\partial x} \\ \frac{\partial N_1}{\partial y} & \frac{\partial N_2}{\partial y} & \cdots & \frac{\partial N_p}{\partial y} \\ \frac{\partial N_1}{\partial z} & \frac{\partial N_2}{\partial z} & \cdots & \frac{\partial N_p}{\partial z} \end{bmatrix} \tag{22}$$

- *Step 4*: The element equations (12) can be assembled in the usual manner to obtain the overall equations as

$$[\underline{K_3}]\dot{\vec{T}} + [\underline{K}]\vec{T} = \vec{P} \tag{23}$$

where

$$[\underline{K_3}] = \sum_{e=1}^{E} [K_3^{(e)}] \tag{24}$$

$$[\underline{K}] = \sum_{e=1}^{E} [[K_1^{(e)}] + [K_2^{(e)}]] \tag{25}$$

and

$$\overset{\leftrightarrow}{\underline{P}} = \sum_{e=1}^{E} \vec{P}^{(e)} \tag{26}$$

- *Step 5*: Eq. (23) have to be solved after incorporating the boundary conditions specified over S_1 and the initial conditions.

3.4. Heat transfer problems with radiation

The inclusion of radiation boundary condition becomes the heat transfer problem in a nonlinear one. Hence an iterative method procedure has to be adopted to find the finite element solution of the problem. If the heat flux is specified on the surface and if both convection and radiation losses take place from the surface, the boundary conditions of the problem can be expressed as [9]

$$k_x \frac{\partial T}{\partial x} + k_y \frac{\partial T}{\partial y} + k_z \frac{\partial T}{\partial z} + h(T - T_\infty) + q + \sigma\varepsilon(T^4 - T_\infty^4) = 0 \text{ on the surface} \tag{27}$$

For convenience, we define [10]:

$$h_r = \sigma\varepsilon(T^2 + T_\infty^2)(T + T_\infty) \tag{28}$$

so that Eq. (27) can be expressed as

$$k_x \frac{\partial T}{\partial x} + k_y \frac{\partial T}{\partial y} + k_z \frac{\partial T}{\partial z} + h(T - T_\infty) + q + h_r(T - T_\infty) = 0 \text{ on the surface} \tag{29}$$

The inclusion of the convection term $h(T - T_\infty)$ in the finite analysis resulted in the matrix [10,11]:

$$[K_2^{(e)}] = \int_{S_3^{(e)}} h[N]^T[N]\mathrm{d}S_3$$

and the vector

$$\vec{P}_3^{(e)} = \int_{S_3^{(e)}} hT_\infty[N]^T\mathrm{d}S_3$$

Assuming, for the time being, that h_r is independent of the temperature T, and proceeding as in the case of the term $h(T - T_\infty)$, we obtain the additional matrix:

$$[K_4^{(e)}] = \int_{S_4^{(e)}} h_r[N]^T[N]\mathrm{d}S_4 \tag{30}$$

and the additional vector

$$\vec{P}_4^{(e)} = \int_{S_4^{(e)}} h_r T_\infty[N]^T\mathrm{d}S_4 \tag{31}$$

to be assembled in generating the matrix $[\underline{K}]$ and the vector $\vec{P}$, respectively. In Eqs. (30) and (31), $S_4^{(e)}$ denotes the surface of the element e from which radiation loss takes place.

4. Numerical simulation method

4.1. General remarks

The above governing equations are discretized by the finite element method (FEM) [14] and then the thermal behavior of the internal light concrete multi-holed brick is optimized [4,5]. The procedure of optimization is based on the design of experiment (DOE) [15,16], which is a technique used to determine the location of sampling points. This technique tries to locate the sampling points such that the space of random input parameters is explored in the most efficient way, or obtain the required information with a minimum of these points. Sample points in efficient locations will not only reduce the required number of points, but also increase the accuracy of the response surface that is derived from the results. In this paper we use a custom-made design points, according to the experimental tests.

4.2. Experimental determination of the light concrete thermal conductivity

In order to study the thermal behavior of the brick, we have determined in the laboratory the relationship between the light concrete's density and its thermal conductivity.

With this aim, five tests were carried out corresponding to five different compositions (termed A, B, C, D, and E, respectively) of the light concrete according to the UNE-92-202-89 rule [17] (see Table 4 below).

The experimental values of the thermal conductivity versus density for the previous different compositions of the light concrete are shown in Table 5.

In order to use the relationship between thermal conductivity and density in the subsequent optimization process, it was necessary to carry out the fitting of the experimental

Table 4
Composition of the light concrete

Composition	Lightweight aggregate [kg]	Sand [kg]	Cement [kg]	Water [$m^3 \times 10^{-3}$]
A	280	208	180	108
B	308	390	170	100
C	336	571	158	90
D	280	952	128	120
E	280	952	168	80

Table 5
Experimental results of the thermal conductivity versus density

Composition	Density [kg/m^3]	Real conductivity λ_t [W/m K]	Estimated conductivity λ_e [W/m K]
A	660	0.151	0.160
B	800	0.19	0.173
C	1040	0.219	0.223
D	1220	0.269	0.282
E	1330	0.337	0.327

results (see Fig. 4). The best fitting was the following one, with a correlation coefficient of 0.97:

$$\lambda_e = C_1 \times \rho^2 + C_2 \times \rho + C_3 \quad (32)$$

being $C_1 = 2.922 \times 10^{-7}$, $C_2 = 3.320 \times 10^{-4}$, and $C_3 = 2.521 \times 10^{-1}$.

For the mortar conductivity, three different values have been taken [2,3], according to Table 6:

4.3. Two-dimensional finite element models, mesh-independence validation and results

In order to check the thermal performance of the different types of bricks ($N1$–$N4$), four walls (one per each type of brick) have been considered. Each one of them is composed of five bricks as it is shown in Fig. 5.

Then, we have built the two-dimensional finite element model. For the modeling of this problem, we have used two-dimensional 8-node quadrilateral finite elements for the solid area of bricks and one-dimensional 3-node (plus an extra node) finite elements for the recesses of bricks (see Fig. 6 below) [18].

In the model, the following thermal conditions are considered: a 10 W/m^2 heat flow in the internal wall side, a 25 W/m^2 K external film coefficient and a 273 K ambient temperature.

In our preliminary computation, mesh-independence of the solution has been examined for the most complex $N4$ hollow brick in which all processes of heat transfer have been considered. Five sets of the mesh sizes have been checked ranging from 4 to 14 mm. The results of the equivalent thermal conductivity are shown in Fig. 8. Comparing a 9 mm size mesh with a 4 mm size mesh (see Fig. 7), we can observed that increasing the mesh size there is only

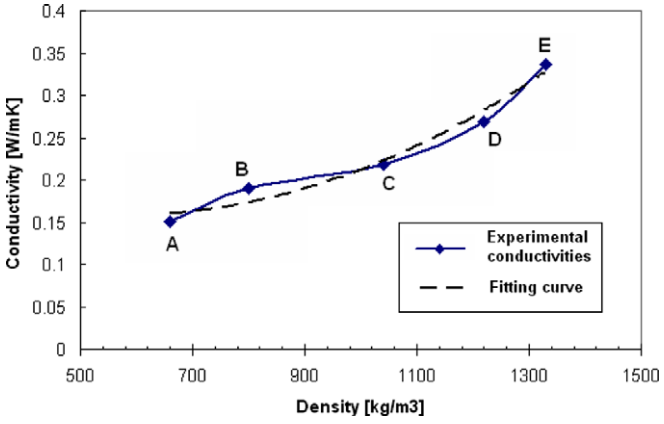

Fig. 4. Experimental results and fitting curve of conductivity vs. density.

Table 6
Mortar thermal conductivities

	Conductivity [W/m K]
Insulating mortar	0.3
Light mortar	1.0
Ordinary mortar	1.4

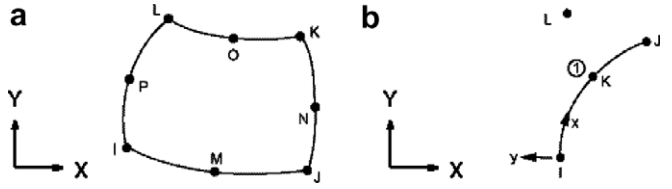

Fig. 6. Finite elements: (a) 8-node quadrilateral and (b) one-dimensional 3-node (plus an extra node) elements.

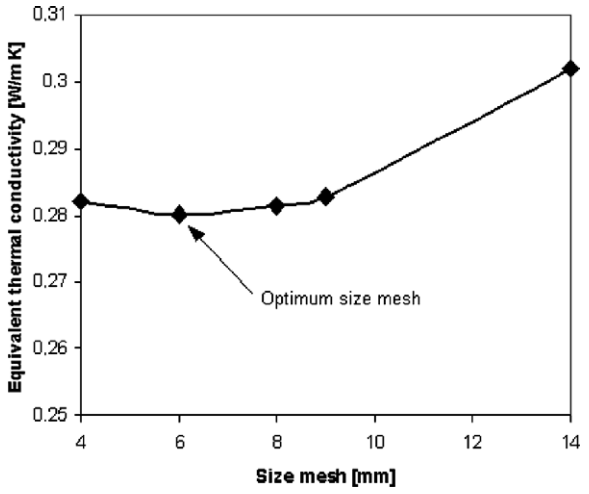

Fig. 7. Validation of mesh independence.

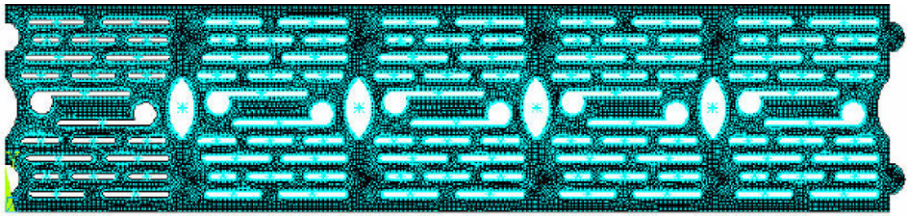

Fig. 5. Two-dimensional wall.

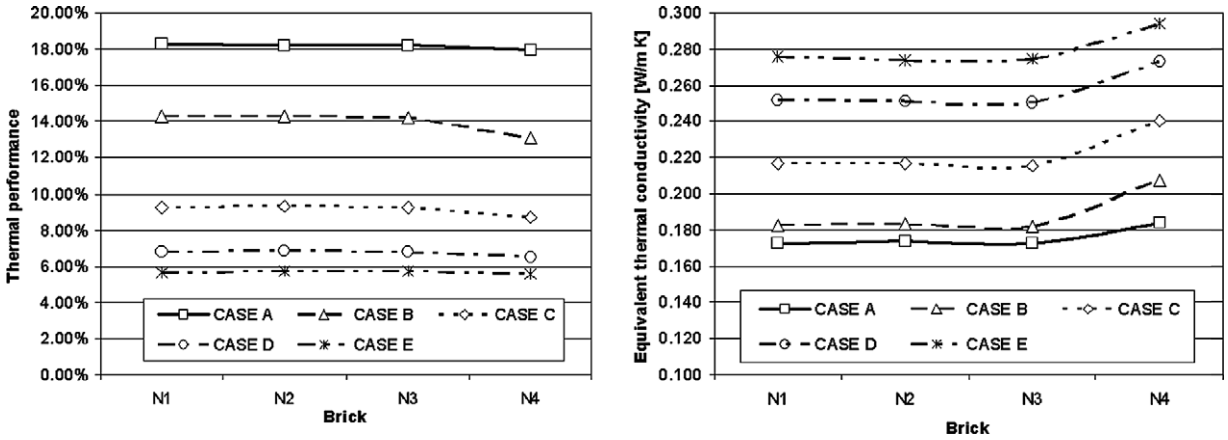

Fig. 8. Mass overall thermal efficiency (left) and equivalent thermal conductivity (right) for the different cases analyzed.

no more than 0.2% difference in the equivalent thermal conductivity. In order to reduce the truncation and round-off errors as well as the computational effort, we have chosen the optimum mesh size of 6 mm in the subsequent simulations.

Table 7
Numerical results for the mass overall thermal efficiency, $e_{\text{thermal\_}p}$, in percentage (m^2 K/W/kg)

CASE/brick	$N1$ (%)	$N2$ (%)	$N3$ (%)	$N4$ (%)
Case A	18.26	18.21	18.22	17.95
Case B	14.26	14.25	14.25	13.12
Case C	9.24	9.28	9.25	8.71
Case D	6.77	6.83	6.79	6.54
Case E	5.67	5.73	5.69	5.57
Average	10.84	10.86	10.84	10.38

Table 8
Numerical results for the equivalent thermal conductivity, $\lambda_{\text{equivalent}}$ (W/m K)

Case/brick	$N1$	$N2$	$N3$	$N4$
Case A	0.173	0.174	0.173	0.184
Case B	0.182	0.183	0.182	0.207
Case C	0.216	0.217	0.216	0.240
Case D	0.252	0.251	0.250	0.273
Case E	0.276	0.274	0.274	0.294

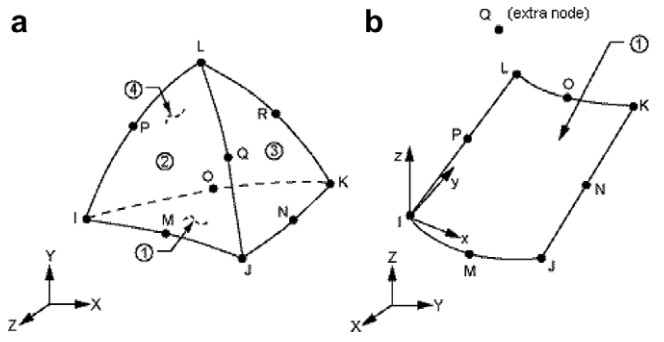

Fig. 9. Three-dimensional finite elements: (a) 10-node tetrahedral thermal solid and (b) thermal surface element.

The determination of the thermal efficiency of a wall is based on the following expressions [19–21]:

$$U = \frac{q/A}{\Delta T} \tag{33}$$

$$R_{\text{tot}} = \frac{1}{U} + R_{\text{si}} + R_{\text{se}} \tag{34}$$

$$e_{\text{thermal\_}p} = \frac{R_{\text{tot}}}{M} \tag{35}$$

$$\lambda_{\text{equivalent}} = \frac{e}{\frac{1}{U} + R_{\text{si}} + R_{\text{se}}} \tag{36}$$

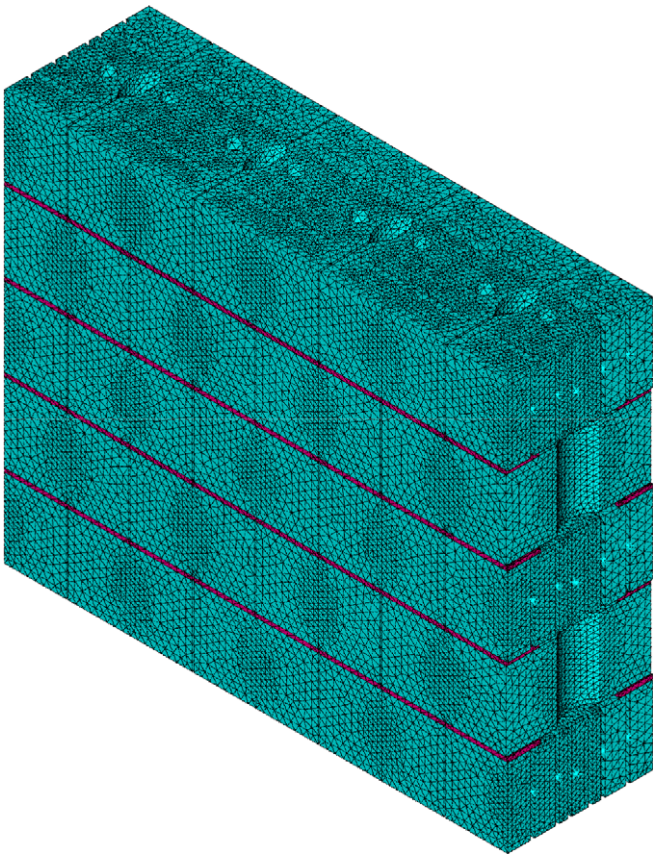

Fig. 10. Three-dimensional finite element model.

Fig. 8 (left) shows the mass overall thermal efficiencies for all analyzed cases, and it reveals that the differences between them are very small, being the brick *N*4 the worst of them. From numerical results in Table 7, we can see that

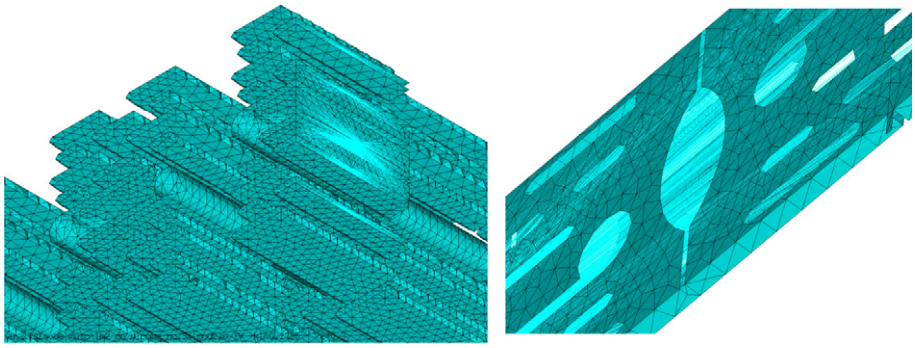

Fig. 11. Mesh of thermal surface elements: vertical mesh in recesses (left) and horizontal mesh in holes between the bricks and mortar (right).

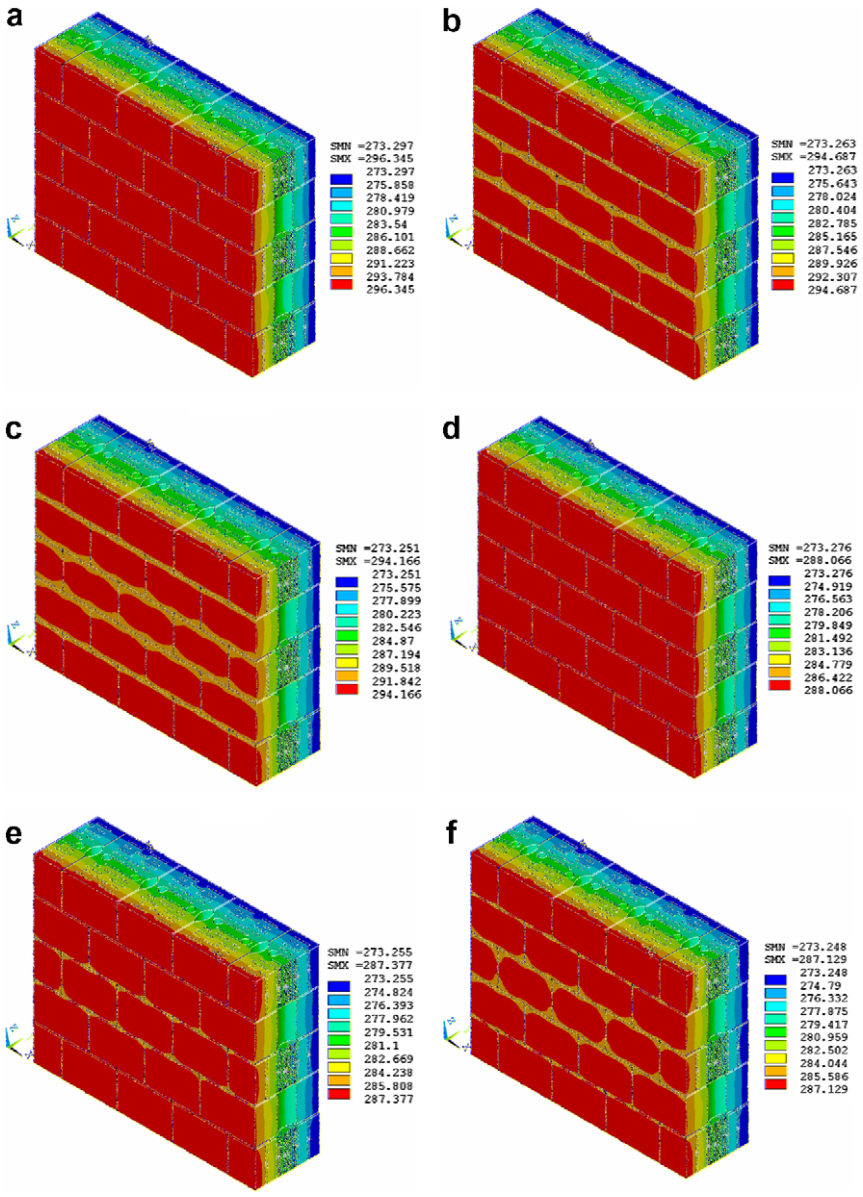

Fig. 12. Temperature distribution in walls for the following cases: (a) Case A, insulating mortar; (b) Case A, light mortar; (c) Case A, ordinary mortar; (d) Case E, insulating mortar; (e) Case E, light mortar and (f) Case E, ordinary mortar.

the best brick from the thermal point of view is the brick *N*2, since its average value (10.86%) is the biggest one.

On the one hand, we show the numerical results for the equivalent thermal conductivity in Table 8. From the point of view of this parameter the best bricks are *N*1, *N*2 and *N*3 with small differences between them (see Fig. 8 right). On the other hand, this behaviour corresponding to intermediate bricks between massive and lighter bricks [2].

The differences between thermal properties of bricks *N*1, *N*2 and *N*3 are very small (see Tables 7 and 8). However, it is necessary to take into account additional considerations, such as the ergonomics (or human factors), that is, the application of scientific information to the design of objects, systems and environment for human use. In this case, aspects such as the total mass and the shape of the brick are very important. In this way, the brick has to be well designed [22] in order to maximize productivity by reducing operator fatigue and discomfort. The brick *N*2 is the lightest one and it presents the best grip. As a consequence of these previous results, then we carry out the three-dimensional thermal analysis of the brick *N*2 by means of the finite element method in the following section.

Table 9
Numerical results

Case	λ_e (W/m K)	λ_{mortar} (W/m K)	U (W/m^2 K)	R_{tot} (m^2 K/W)	λ_{equiv} (W/m K)
Case 1	0.160	0.300	0.466	2.189	0.160
Case 2	0.160	1.000	0.511	2.011	0.174
Case 3	0.160	1.400	0.526	1.956	0.179
Case 4	0.173	0.300	0.488	2.098	0.167
Case 5	0.173	1.000	0.533	1.935	0.181
Case 6	0.173	1.400	0.549	1.883	0.186
Case 7	0.223	0.300	0.567	1.828	0.191
Case 8	0.223	1.000	0.612	1.706	0.205
Case 9	0.223	1.400	0.629	1.665	0.210
Case 10	0.282	0.300	0.653	1.610	0.217
Case 11	0.282	1.000	0.698	1.517	0.231
Case 12	0.282	1.400	0.715	1.485	0.236
Case 13	0.327	0.300	0.714	1.486	0.236
Case 14	0.327	1.000	0.759	1.408	0.249
Case 15	0.327	1.400	0.777	1.380	0.254

4.4. Three-dimensional finite element models and results

We have built a three-dimensional finite element model of a wall made of *N*2 bricks and mortar (see Fig. 2 above). For the modeling of bricks and mortar we have used solid type tetrahedral finite elements with 10 nodes. In order to simulate the convection and radiation phenomena in the recesses, surface elements with 9 nodes (8 nodes + 1 extra node included) have been used (see Fig. 9 below) [18].

The complete finite element model of the wall can be appreciated in Fig. 10. A detail of the thermal surface elements is shown in Fig. 11. In this model we have considered the same thermal conditions than the two-dimensional model. Keeping in mind the same geometrical configuration of the brick *N*2, varying the thermal conductivities both in the brick and in the mortar, we present as results the temperature distribution in the wall (see Fig. 12).

The results obtained by FEM are processed in order to obtain the thermal characteristic values of the walls [2–5,21].

Comparing to the numerical results (Table 9 and Fig. 13) with the CTE rule requirements [1] (see Table 3 above), we see that the thermal performance of the new light concrete hollow bricks analyzed is in agreement with the objective values established in the CTE rule. At the same time, we have calculated the distribution according to climatic zones for the 52 Spanish capitals as well as the percentage of bricks fulfilling the CTE rule requirements (see Fig. 14).

After examining the results obtained numerically, it can be assumed that the optimization procedure constitutes a reasonable approach to choose the appropriate type of brick that satisfies the CTE rule requirements. The finite element model reproduces quite accurately the heat transfer in walls made of lightweight aggregate concrete with open structure and complex shapes with holes.

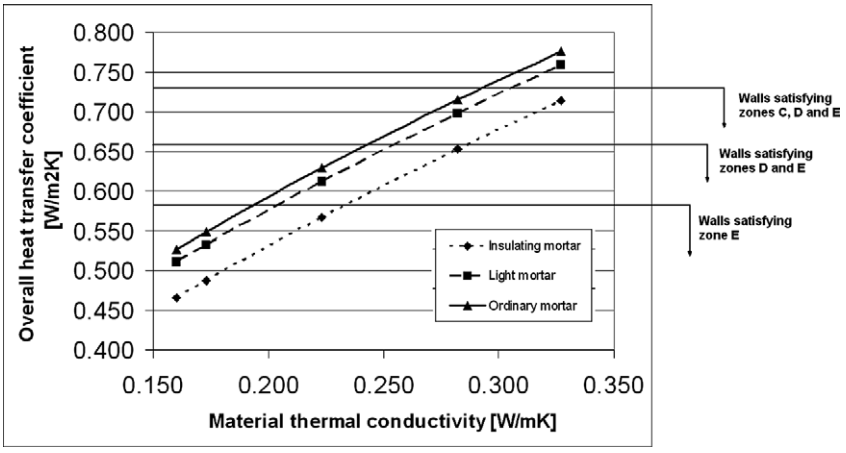

Fig. 13. Overall heat transfer coefficient versus material thermal conductivity, for the fifteen cases analyzed above and walls that satisfy the CTE requirements.

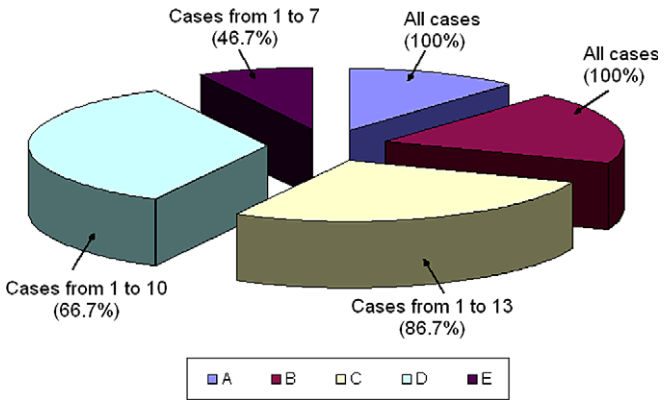

Fig. 14. Climatic zones distribution of Spanish capitals and kind of walls (cases analyzed) that satisfy the requirements of thermal performance according to the CTE rule: zone A (six capitals and all cases analyzed), zone B (10 capitals and all cases analyzed), zone C (14 capitals and 86.7% of cases analyzed), zone D (18 capitals and 66.7% of cases analyzed) and zone E (four capitals and 46.7% of cases analyzed).

5. Conclusions

In this work, the finite element method is used for finding approximate solution of the heat transfer equation, both in two and three-dimensional models. In the first place, the numerical thermal analysis technique (FEM) has been carried out to study four different kinds of walls in two dimensions, made up of five compositions of light concrete hollow bricks, according to the experimental fitted results. With the increase of the length, size and distribution of the holes, it is possible to modify the thermal performance of the bricks. On the basis of the mass overall thermal efficiency and the equivalent thermal conductivity, we have selected the best candidate from the thermal point of view.

Secondly, we have carried out the three-dimensional finite element analysis for the best candidate, varying the mortar and brick conductivities obtained from experimental tests in laboratory. The equivalent thermal conductivity depends on three heat transfer processes: the heat conduction through the solid brick and mortar, the radiation between recess surfaces and the natural convection in vertical and horizontal holes. According to the numerical results, we see that the overall heat transfer coefficient depends on both the material and mortar thermal conductivities. In order to select the appropriate wall satisfying the CTE requirements, Fig. 13 shows three well-defined cross sections.

Finally, we have compared the thermal performance of the different types of bricks, according to the CTE Spanish rule requirements showing the results obtained for the 52 Spanish capitals in Fig. 14.

Overall heat transfer coefficient increases if the mortar and material conductivities increase. The bigger mass overall thermal efficiency, the better thermal insulation and the lower wall's weight. Therefore, the support structure of these walls will be subjected to smaller dead loads and the best brick from the average mass overall thermal efficiency point of view was the brick *N*2.

To define the geometry of a hollow brick like this is very cumbersome using an analysis program by finite elements. For this reason, a three-dimensional parametric design program was used in order to make up the five hollow bricks.

The finite element model reproduces quite accurately the heat transfer mechanism in walls made up of lightweight aggregate concrete with open structure and complex shapes of recesses. In this sense, the key step in engineering analysis is therefore choosing appropriate mathematical models. These models will clearly be selected depending on what phenomena are to be predicted, and it is most important to select mathematical models that are *reliable* and *effective* in predicting the quantities sought [10–14].

As final conclusion, for housing and industrial structures there is a great interest in light building materials with good physical material performance, with respect to an energy conscious and ecological design, which fulfil all strength and serviceability requirements. From this point of view, the designer can use the results shown in the previous section in order to obtain the best wall configuration according to the CTE rule requirements.

Acknowledgements

The authors wish to acknowledge the financial support provided by the Department of Construction at University of Oviedo and the MAXIT Group. We also thank to Swanson Analysis Inc. for the use of ANSYS University Intermediate program and AST Simulation Ltd. for the use of ANSYS Mechanical.

References

[1] CTE Spanish rule – DB-HE Document: Energy Saving, Ministry of Buildings, March 2006.
[2] J.J. del Coz Díaz, P.J. García Nieto, C. Betegón Biempica, M.B. Prendes Gero, Analysis and optimization of the heat-insulating light concrete hollow brick walls design by the finite element method, Appl. Thermal Eng. 27 (2007) 1445–1456.
[3] J.J. del Coz Díaz, P.J. García Nieto, A. Martín Rodríguez, A. Lozano Martínez-Luengas, C. Betegón Biempica, Non-linear thermal analysis of light concrete hollow brick walls by the finite element method and experimental validation, Appl. Thermal Eng. 26 (8–9) (2006) 777–786.
[4] S. Lorente, M. Petit, R. Javelas, Simplified analytical model for thermal transfer in vertical hollow brick, Energ. Build. 24 (2) (1996) 95–103.
[5] C. Vasile, S. Lorente, B. Perrin, Study of convective phenomena inside cavities coupled with heat and mass transfers through porous media—application to vertical hollow bricks—a first approach, Energ. Build. 28 (3) (1998) 229–235.
[6] F.P. Incropera, D.P. DeWitt, Introduction to Heat Transfer, Wiley, New York, 2001.
[7] F. Kreith, M.S. Bohn, Principles of Heat Transfer, Thomson-Engineering, New York, 2000.
[8] A.F. Mills, Heat Transfer, Prentice Hall, New York, 1998.
[9] R. Siegel, J.R. Howell, J. Howell, Thermal Radiation Heat Transfer, Taylor & Francis Group, 2001.
[10] K. Bathe, Finite Element Procedures, Prentice-Hall, Englewoods Cliffs, New Jersey, 1998.

[11] O.C. Zienkiewicz, R.L. Taylor, The Finite Element Method, McGraw-Hill Book Company, United Kingdom, 1991.
[12] R.D. Cook, D.S. Malkus, M.E. Plesha, R.J. Witt, Concepts and Applications of Finite Element Analysis, Wiley, New York, 2001.
[13] T. Chandrupatla, A. Belegundu, Introduction to Finite Element in Engineering, Prentice-Hall, Englewood Cliffs, New Jersey, 1991.
[14] S.C. Brenner, L.R. Scott, The Mathematical Theory of Finite Element Methods, Springer-Verlag, New York, 2002.
[15] J. Antony, Design of Experiments for Engineers and Scientists, Butterworth-Heinemann, New York, 2003.
[16] D.C. Montgomery, Design and Analysis of Experiments, John Wiley & Sons, New York, 2004.
[17] UNE 92-202-89 Rule, Thermal Insulation Materials. Determination of Thermal Conductivity. Heat Flow Meter Method, AENOR, Madrid, 1989.
[18] E. Madenci, I. Guven, The Finite Element Method and Applications in Engineering using ANSYS, Springer, Berlin, 2005.
[19] EN-1934, Thermal Performance of Buildings – Determination of Thermal Resistance by Hot Box Method using Heat Flow Meter – Masonry, CEN, Brussels, 1998.
[20] UNE-EN-1745, Masonry and Masonry Products. Methods for Determining Design Thermal Values, AENOR, Madrid, 2002.
[21] UNE-EN ISO 6946, Elements and Construction Components. Resistance and Thermal Transmittance: Calculation Method, AENOR, Madrid, 1997.
[22] J.R. Wilson, N. Corlett, Evaluation of Human Work, TF-CRC, New York, 2005.